

On the photo- and thermally-induced darkening phenomena in $\text{As}_{40}\text{S}_{40}\text{Se}_{20}$ amorphous chalcogenide thin films

E Márquez[†], J M González-Leal[†], R Prieto-Alcón[†],
R Jiménez-Garay[†] and M Vlcek[‡]

[†] Departamento de Física de la Materia Condensada, Facultad de Ciencias,
Universidad de Cádiz, 11510-Puerto Real (Cádiz), Spain

[‡] Department of General and Inorganic Chemistry, Faculty of Chemical Technology,
University of Pardubice, 53210-Pardubice, Czech Republic

E-mail: emilio.marquez@uca.es

Received 29 April 1999

Abstract. Annealing (in vacuum) at a temperature near the glass transition temperature and exposure (in air) with bandgap light of thermally-evaporated $\text{As}_{40}\text{S}_{40}\text{Se}_{20}$ amorphous chalcogenide thin films, were found to be accompanied by structural changes, which lead to changes in the refractive index and shifts in the optical absorption edge. Indications of photo-oxidation were found after light exposure in air. An optical characterization method, based on the transmission spectra at normal incidence of uniform thickness thin films, has been used to obtain the optical constants and the film thicknesses corresponding to the virgin, annealed and exposed $\text{As}_{40}\text{S}_{40}\text{Se}_{20}$ samples. The dispersion of the refractive index is discussed in terms of the single-oscillator Wemple–DiDomenico model. The optical absorption edges are described using the ‘non-direct transition’ model proposed by Tauc.

1. Introduction

Chalcogenide glass thin films are a subject of systematic research because of the changes in physical and chemical properties, which occur in samples after illumination or annealing [1–11]. These photo- and thermally-induced effects may be either irreversible or reversible, and offer the possibility of using amorphous chalcogenide semiconductors for high-density information storage, high-resolution display devices and fabrication of diffractive optical elements [12–14]. In particular, As–S–Se glasses are attractive candidates for all these technological applications [13, 14].

The aim of the present paper is to study the changes in the optical properties of $\text{As}_{40}\text{S}_{40}\text{Se}_{20}$ amorphous chalcogenide thin films, after annealing at a temperature relatively near the glass transition temperature, T_g , or after illumination with bandgap light. As-deposited, thermal-darkened and photo-darkened films have been optically characterized from their corresponding transmission spectra at normal incidence, using the accurate method of the envelope curves suggested by Swanepoel for thin films of uniform thickness [15], which has been successfully used by the authors in previous works [16, 17]. The results obtained have been compared with those found in the literature for amorphous chalcogenide films of the related binary stoichiometric compositions $\text{As}_{40}\text{S}_{60}$ (As_2S_3) and $\text{As}_{40}\text{Se}_{60}$ (As_2Se_3) [2]. The lack of data in the literature concerning the optical characterization of thin films of ternary chalcogenide glasses confirms the significance of the present study.

2. Experimental details

Thin films were prepared by vacuum evaporation of the powdered, melt-quenched glassy material, onto clean glass substrates (microscope slides). The thermal evaporation process was performed inside a coating system (Tesla Corporation, model UP-858), at a pressure of about 10^{-5} Torr, which is typically applied for vacuum evaporation of chalcogenide glasses. During the deposition process, the substrates were suitably rotated by means of a planetary rotation system, in order to obtain homogeneous films of uniform thickness. The deposition rate was $\approx 6\text{--}8$ nm s^{-1} , as measured by the dynamic weighing method. This deposition rate results in a film chemical composition which is very close to that of the starting bulk material. The composition of the chalcogenide films was found to be $\text{As}_{39.8\pm 0.5}\text{S}_{39.9\pm 0.6}\text{Se}_{20.3\pm 0.3}$, by means of electron microprobe x-ray analysis (Jeol, model JSM-820). Some as-deposited $\alpha\text{-As}_{40}\text{S}_{40}\text{Se}_{20}$ films were annealed at $\approx 160^\circ\text{C}$ for around 24 h under a vacuum of 10^{-3} Torr (the glass transition temperature, measured by a modulated differential scanning calorimetry experiment [18], was $\approx 199^\circ\text{C}$). Other films were illuminated in air, by a 500 W Hg arc lamp (Oriel, model 6285), through an infrared (IR)-cut filter, providing broadband white light, with a very high ultraviolet (UV) output, and with a light intensity of ≈ 40 mW cm^{-2} . 3 h of illumination was found to be enough to reach the saturation state. The 200–900 nm spectral irradiance curve of the Hg arc lamp is displayed in figure 1, along with that corresponding

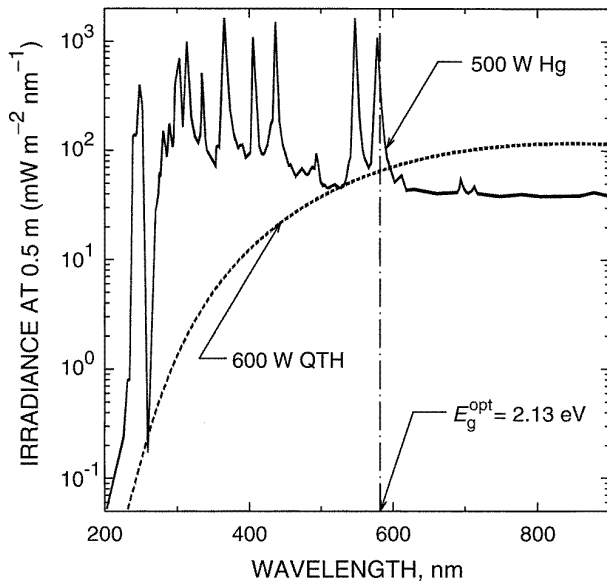


Figure 1. Spectral irradiance curve of the 500 W Hg lamp and that corresponding to a 600 W QTH lamp, for the sake of comparison [19].

to a 600 W quartz tungsten halogen (QTH) lamp [19]. Note the much higher output in the UV spectral region, for the case of the Hg lamp, in comparison with a typical ‘white’ light source.

The lack of crystallinity in the as-deposited films was verified by x-ray diffraction (XRD) measurements (Philips, model PW-1820). After annealing or illumination, the XRD analysis was also performed in order to study the changes occurring during these two processes. The optical transmission spectra were measured by a double-beam UV/Vis/NIR spectrophotometer, with automatic computer-data acquisition (Perkin-Elmer, model Lambda-19), and the wavelength range analysed was 400–2500 nm. The transmission measurements were made in various parts of the glass films, scanning the entire sample, and a very good reproduction of the transmission spectrum was generally achieved. The spectrophotometer was set with a suitable slit width of 1 nm, in the UV/Vis spectral region. A surface-profiling stylus (Sloan, model Dektak 3030) was also used to measure independently the film thickness, which was compared with the thickness calculated from the transmission spectrum. The thicknesses of the investigated *a*-As₄₀S₄₀Se₂₀ films were in the range 800–1400 nm. Also, mass measurements were made by a microbalance (Mettler, model AE200) to check possible changes as a consequence of the different treatments. All the optical measurements were performed at room temperature on films previously stored in conditions of continuous darkness.

3. Results and discussion

Figure 2 shows the XRD patterns corresponding to the representative, as-deposited, annealed and illuminated films. A feature of diffraction data of covalently-bonded amorphous solids, which has long been associated with the presence of medium-range order (MRO), is the first sharp diffraction peak (FSDP) occurring at values of the scattering vector

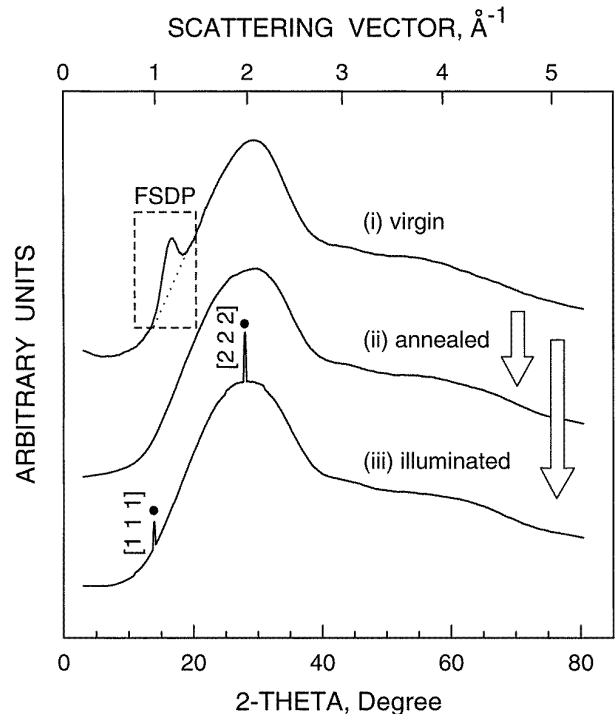


Figure 2. XRD-patterns (Cu $K\alpha$ radiation) of the As₄₀S₄₀Se₂₀ amorphous films: (i) as-evaporated; (ii) annealed at a temperature relatively near T_g ; and (iii) exposed to bandgap radiation. (The data have been smoothed by means of the Savitzky–Golay filter.)

$Q (= 4\pi \sin \theta / \lambda) = 1\text{--}2 \text{ \AA}^{-1}$, depending on the material [2, 20–26]. In the present case, this significant feature appears at $2\theta \approx 17^\circ$, or equivalently at $Q \approx 1.1 \text{ \AA}^{-1}$.

Many attempts have been made to explain the origin of the FSDP in glasses. Elliott [20, 21] has recently proposed a new explanation, in which the FSDP is ascribed to a chemical-order pre-peak (in the concentration–concentration partial structure factor, $S_{cc}(Q)$, in the Bhatia–Thornton formalism [27]), due to interstitial volume around cation-centred structural units. This association of the FSDP with correlations involving interstitial voids plausibly explains the anomalous behaviour of this peak as a function of temperature and pressure. It can also be seen in figure 2 that, after both the annealing and the illumination of the as-deposited samples, the FSDP disappears. These experimental results suggest, according to Elliott’s ideas, a thermal- and a photo-densification of the chalcogenide glass structure, i.e. a clear diminution of the interstitial volume around the As-centred structural units. It is important to note that, in the case of As₄₀S₆₀ and As₄₀Se₆₀ binary glass thin films [2, 3], the intensity profile of the FSDP decreases, broadens and shifts to higher angle as a consequence of either the annealing or the illumination, but does not entirely disappear.

The optical study of the thermally- and photo-induced changes in *a*-As₄₀S₄₀Se₂₀ thin films, has been carried out, as already stated, using a method suggested by Swanepoel for the case of homogeneous thin layers. An initial estimate of the refractive index of the virgin, annealed and illuminated films was obtained from the expression

$$n_1 = \sqrt{N + \sqrt{N^2 - s^2}} \quad (1a)$$

with s being the refractive index of the substrate, which is independently calculated from the transmission spectrum of the bare substrate (see [15]), and N as

$$N = 2s \frac{T_M - T_m}{T_M T_m} + \frac{s^2 + 1}{2} \quad (1b)$$

where T_M and T_m are the transmission values corresponding to the tangent points between the upper and lower envelopes, respectively, and the experimental transmission spectrum. The top and bottom envelopes were very carefully computer-drawn using software created by McClain *et al* [28].

A first estimate of the film thickness, d_1 , was obtained using the relationship

$$d_1 = \frac{\lambda' \lambda''}{4(n_1'' \lambda' - n_1' \lambda'')} \quad (2)$$

where n_1' and n_1'' are the refractive indices for two adjacent tangent points, having wavelengths λ' and λ'' , respectively. The above expression is derived from the well known equation for the interference fringes

$$2nd = m\lambda \quad (3)$$

with m being an integer or a half-integer for an upper or a lower tangent point, respectively. It should be pointed out that, owing to the optical absorption, this particular equation is not valid at the interference maxima and minima, but is valid at the tangent points referred to [29]. Using equation (3), new more precise values of the refractive index and the film thickness were determined by a procedure which was explained in detail in [15]. Figure 3 shows a typical optical transmission spectrum corresponding to a representative, as-deposited $\text{As}_{40}\text{S}_{40}\text{Se}_{20}$ film, along with its upper and lower envelopes, and also the transmission of the bare glass substrate, T_s .

The thicknesses of the virgin, annealed and illuminated samples, calculated using the optical characterization method outlined above, are listed in table 1. In all cases, the thicknesses determined by mechanical measurements were in excellent agreement, indeed, with those obtained by the envelope method—the differences being always less than 2%. The decrease in the thickness of the $\text{As}_{40}\text{S}_{40}\text{Se}_{20}$ layers due to annealing, $\approx 4.3\%$, is a clear sign of a thermal-densification process [7]. Similarly, the exposure of the samples to bandgap light also causes a significant decrease in the as-deposited film thickness, $\approx 5.2\%$, because the illumination takes the structure of the virgin film also closer to the network structure of the bulk glass [3]. On the other hand, changes in the masses of the thermal- and photo-darkened films, measured by the microbalance, were not observed.

In figure 4 the refractive indices are plotted as a function of photon energy. In this figure it can be seen that this optical constant increases upon annealing or illumination; a similar behaviour has been found by De Neufville *et al* [2] in binary stoichiometric $\text{As}_{40}\text{S}_{60}$ and $\text{As}_{40}\text{Se}_{60}$ films. The dispersion of the refractive index has been analysed in terms of the Wemple–DiDomenico model [30, 31], which is based on the single-oscillator formula

$$n^2(\hbar\omega) = 1 + \frac{E_0 E_d}{E_0^2 - (\hbar\omega)^2} \quad (4)$$

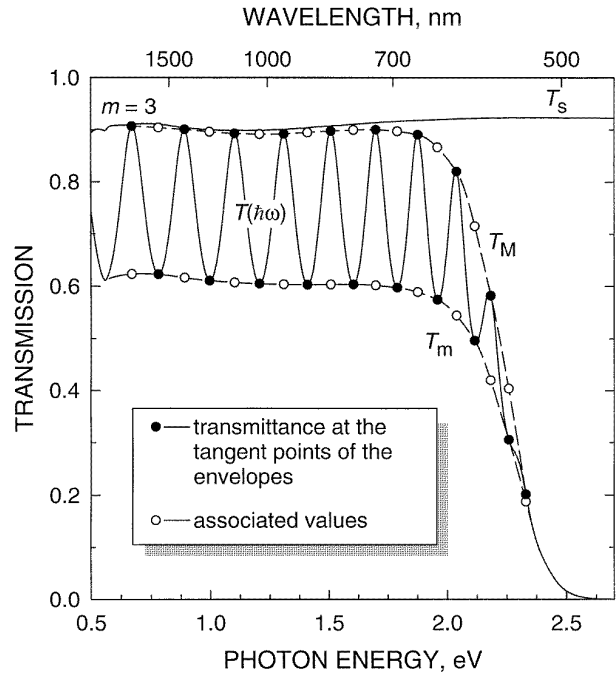


Figure 3. Experimental optical transmission spectrum, $T(\hbar\omega)$, as a function of photon energy, of a representative as-deposited $\text{As}_{40}\text{S}_{40}\text{Se}_{20}$ chalcogenide film. T_M and T_m are the upper and lower envelope curves, respectively, and T_s is the transmission of the bare substrate. The order number, m , shown is that corresponding to the first tangent point.

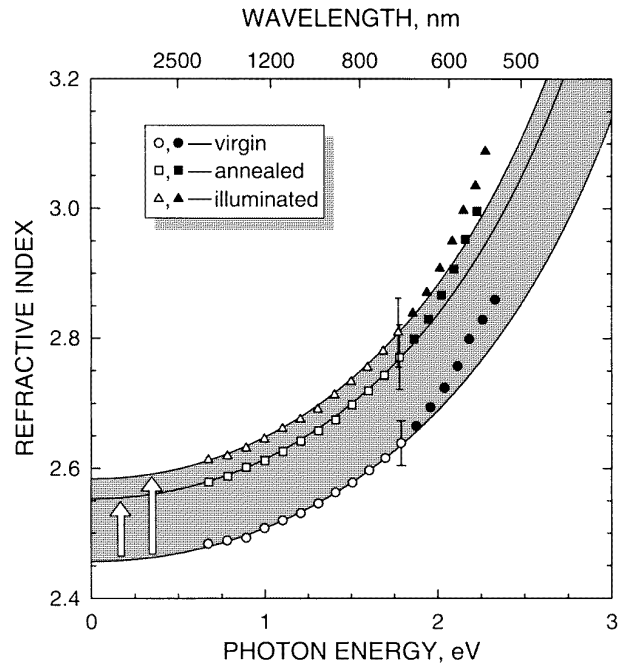


Figure 4. Refractive index as a function of photon energy, for the three states of the $\text{As}_{40}\text{S}_{40}\text{Se}_{20}$ sample. The curves have been drawn from the Wemple–DiDomenico dispersion relationship.

where \hbar is Dirac's constant ($= h/2\pi$, h being Planck's constant), $\hbar\omega$ is the photon energy, E_0 is the single-oscillator energy and E_d is the dispersion energy. By plotting $(n^2 - 1)^{-1}$ against $(\hbar\omega)^2$ and fitting a straight line as shown in figure 5,

Table 1. Values of the film thickness (d), along with their standard deviations, σ_{n-1} , and the corresponding relative errors. Also included are the single-oscillator energy or Wemple–DiDomenico ‘gap’ (E_0), dispersion energy (E_d), static refractive index ($n(0)$), Tauc slope ($B^{1/2}$), Tauc optical gap (E_g^{opt}), gap ratio (E_0/E_g^{opt}), an alternative option for the optical gap (E_{04}), and the slope parameter of the Urbach region (E_e). The errors of all these optical quantities have been directly derived from the values of each σ_{n-1} , associated with the two straight-line parameters obtained by the least-squares fit.

| State of the sample | d (nm) | E_0 (eV) | E_d (eV) | $n(0)$ | $B^{1/2}$ (cm ^{-1/2} eV ^{-1/2}) | E_g^{opt} (eV) | E_0/E_g^{opt} | E_{04} (eV) | E_e (meV) |
|---------------------|------------------|-------------|--------------|---------------|--|------------------|-----------------|---------------|-------------|
| Virgin | 1116 ± 15 (1.3%) | 4.57 ± 0.04 | 22.99 ± 0.18 | 2.457 ± 0.001 | 783 ± 2 | 2.13 ± 0.01 | 2.15 ± 0.03 | 2.35 ± 0.01 | 117 ± 1 |
| Thermal-darkened | 1068 ± 19 (1.8%) | 4.29 ± 0.02 | 23.68 ± 0.13 | 2.553 ± 0.001 | 839 ± 2 | 2.09 ± 0.01 | 2.05 ± 0.02 | 2.29 ± 0.01 | 108 ± 1 |
| Photo-darkened | 1058 ± 20 (1.9%) | 4.23 ± 0.03 | 24.04 ± 0.14 | 2.584 ± 0.001 | 828 ± 1 | 2.06 ± 0.01 | 2.05 ± 0.02 | 2.25 ± 0.01 | 118 ± 1 |

E_0 and E_d are directly determined from the slope, $(E_0 E_d)^{-1}$, and the intercept, E_0/E_d , on the vertical axis. However, it must be taken into account that, owing to the optical absorption, the experimental variation in the refractive index clearly departs from that given by equation (4), when the photon energy approaches the optical-gap value (see figure 5) [30, 32]. The values of the dispersion parameters E_0 and E_d , as well as the corresponding static refractive index $n(0)$ (at $\hbar\omega = 0$), for the as-evaporated, annealed and exposed films are listed in table 1. The oscillator energy is an ‘average’ energy gap, and to a very good approximation it scales with the optical-band gap E_g^{opt} , $E_0 \approx 2 \times E_g^{opt}$, as was found by Tanaka [33] investigating well annealed As_xS_{100-x} glass films. Furthermore, E_d also obeys a simple empirical relationship [30, 31]

$$E_d = \beta N_c Z_a N_e \text{ (eV)} \quad (5)$$

where N_c is the coordination number of the cation nearest-neighbour to the anion, Z_a is the formal chemical valency of the anion, N_e is the effective number of valence electrons per anion and $\beta \approx 0.4$ eV for covalent crystalline and amorphous materials.

As a consequence of both annealing and illumination, the oscillator strength increases. Assuming $N_e = (40 \times 5 + 60 \times 6)/60 = 28/3$ and $Z_a = 2$, and that they should not be changed by either of the above-mentioned treatments, it seems reasonable to ascribe such a trend observed in the values of E_d to an increase in the effective cation coordination number N_c . Furthermore, it is well known that the As₂Ch₃ chalcogenides (Ch being a chalcogen atom) consist of two-dimensional structural layers, in which the As-coordination number is three. Therefore, the suggested increase in N_c could be explained in terms of an increase of the interaction between these structural layers, as a consequence of the thermal- and photo-densification phenomena. On the other hand, the changes found in the static refractive index upon annealing, $\Delta n(0) = +0.096 \pm 0.002$, and illumination, $\Delta n(0) = +0.127 \pm 0.002$, are certainly consistent with those reported for low energies (IR-region) by De Neufville *et al* [2], for the particular case of binary As₄₀S₆₀ and As₄₀Se₆₀ films. Similarly to [2], the refractive index increases slightly more after illumination than after annealing. Moreover, it should be pointed out that the refractive indices, corresponding to either annealed

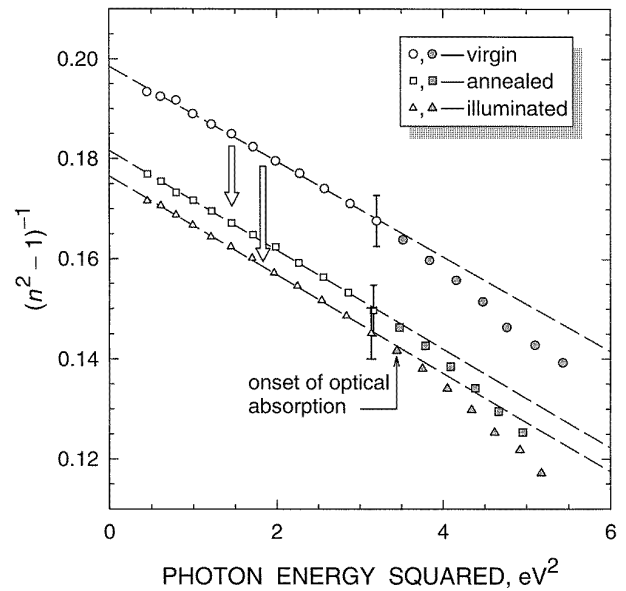


Figure 5. Plot of the refractive-index factor $(n^2 - 1)^{-1}$ versus $(\hbar\omega)^2$, for the as-deposited, thermal- and photo-darkened As₄₀S₄₀Se₂₀ films.

or exposed films, attain values very close to the bulk-glass values [34, 35].

In order to study the thermally- and photo-induced changes in the optical absorption edge of the present thin-film samples, the optical absorbance, x , was derived from the upper envelope, T_M , by means of the following expression [15]:

$$x = \frac{E_M - [E_M^2 - (n^2 - 1)^3(n^2 - s^4)]^{1/2}}{(n - 1)^3(n - s)^2} \quad (6a)$$

where

$$E_M = \frac{8n^2s}{T_M} + (n^2 - 1)(n^2 - s^2). \quad (6b)$$

Once the absorbance, x , and the film thickness, d , were known, the equation $x = \exp(-\alpha d)$ was solved to obtain the absorption coefficient, α . The extinction coefficient, k , was then determined from the relationship $k = \alpha\lambda/4\pi$. The dependence of the absorption coefficient on photon energy is displayed in figure 6, using a semi-logarithmic scale. As can be seen in this figure, the annealing causes a clear shift of

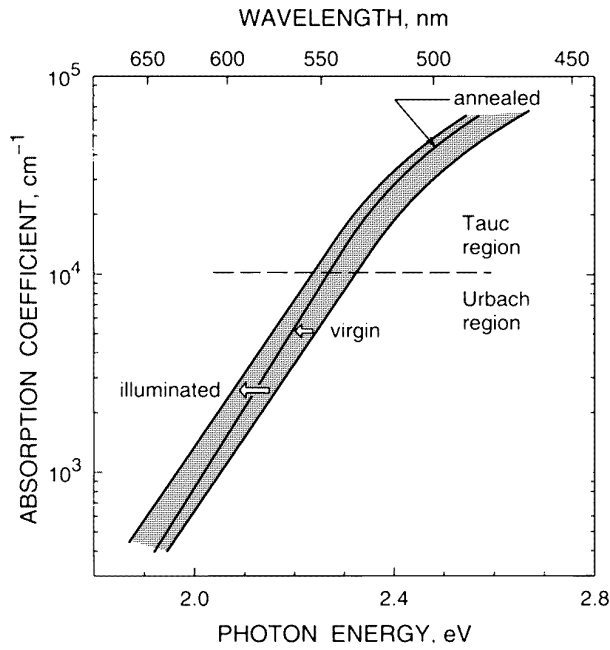


Figure 6. Changes in the optical absorption edge of a representative, as-deposited $\text{As}_{40}\text{S}_{40}\text{Se}_{20}$ film, induced by annealing and illumination: a red shift takes place in both cases.

the optical absorption edge of the as-deposited film to lower energies (i.e. thermal-darkening). Similarly, the exposure to bandgap light also leads to a red shift (i.e. photo-darkening).

In addition, to obtain the thin-film optical gap and determine the nature of the optical transitions involved, the dependence of the absorption coefficient on the photon energy was analysed. According to Tauc [36], it is possible to separate three distinct regions in the optical absorption edge for amorphous semiconductors: the weak absorption tail, the exponential edge region and the high absorption region. The weak absorption region originates from defects and impurities, while the exponential region is strongly related to the structural randomness of the disordered material. Finally, the high absorption region determines the optical energy gap. In the exponential edge region (where $1 \text{ cm}^{-1} \lesssim \alpha \lesssim 10^4 \text{ cm}^{-1}$), the absorption coefficient is governed by the so-called Urbach relationship [36, 37]

$$\alpha(\hbar\omega) = \alpha_0 \exp\left(\frac{\hbar\omega}{E_e}\right) \quad (7)$$

where E_e characterizes the slope of the exponential edge region. Plotting the dependence of $\log \alpha$ versus $\hbar\omega$, as shown in figure 6, should give a straight line. The calculated value of the parameter E_e , the inverse of the slope of the straight line, gives the width of the tails of the localized states at the band gap. The E_e -values found for the virgin, thermal- and photo-darkened $a\text{-As}_{40}\text{S}_{40}\text{Se}_{20}$ films are all listed in table 1.

In the strong absorption region ($\alpha \gtrsim 10^4 \text{ cm}^{-1}$), involving inter-band optical transitions between valence and conduction bands, the absorption coefficient of amorphous semiconductors is given, according to Tauc [36], by the following quadratic relationship:

$$\alpha(\hbar\omega) = B \frac{(\hbar\omega - E_g^{opt})^2}{\hbar\omega} \quad (8)$$

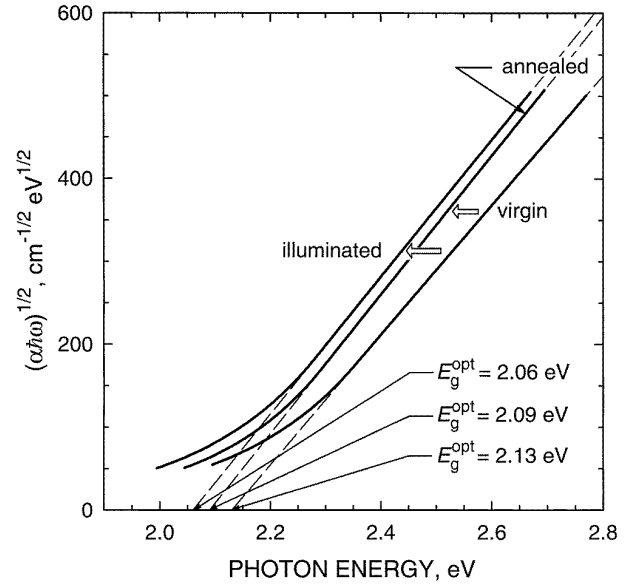


Figure 7. Determination of the optical gap, in terms of Tauc's law, for the as-evaporated, thermal- and photo-darkened $\text{As}_{40}\text{S}_{40}\text{Se}_{20}$ samples.

where B is a constant which depends on the transition probability and E_g^{opt} is the optical energy gap. The values of E_g^{opt} and B can be readily derived from equation (8), by plotting $(\alpha\hbar\omega)^{1/2}$ versus $\hbar\omega$. An excellent fit between the high-energy experimental points and the straight line corresponding to the $(\alpha\hbar\omega)^{1/2}$ versus $\hbar\omega$ plot, shown in figure 7, indicates that non-direct transition is the mechanism responsible for the optical absorption, in the case of the as-deposited, thermal- and photo-darkened $a\text{-As}_{40}\text{S}_{40}\text{Se}_{20}$ layers.

The values of the Tauc gap, E_g^{opt} , and Tauc slope, $B^{1/2}$, as well as the alternative optical gap, E_{04} , which represents the energy at which the absorption coefficient reaches the value of 10^4 cm^{-1} , for the three representative samples, are presented in table 1. The change found in the optical gap E_{04} after annealing was $\Delta E_{04} \approx -0.06 \text{ eV}$, while those reported by De Neufville *et al* [2] for $\Delta E_{04}(\text{As}_{40}\text{S}_{60})$ and $\Delta E_{04}(\text{As}_{40}\text{Se}_{60})$ were both $\approx -0.05 \text{ eV}$. In addition, the decrease in E_{04} upon illumination was $\Delta E_{04} \approx -0.10 \text{ eV}$, and those reported in [2] were $\Delta E_{04}(\text{As}_{40}\text{S}_{60}) \approx -0.07 \text{ eV}$ and $\Delta E_{04}(\text{As}_{40}\text{Se}_{60}) \approx -0.06 \text{ eV}$. Last but not least, one can conclude from the results in table 1 that the E_g^{opt} -values clearly satisfy the relationship $E_0 \approx 2 \times E_g^{opt}$. However, it should be pointed out that this particular relationship between the two gaps was found for well annealed $\text{As}_x\text{S}_{100-x}$ chalcogenide films. This fact could certainly explain why the values of E_0 and E_g^{opt} , corresponding to the samples subjected to the different treatments, present a better agreement with the previous expression (i.e. the ratio E_0/E_g^{opt} is closer to two), than the value corresponding to the as-deposited layer.

Finally, it is important to mention that, similarly to the previous data on exposed $\text{As}_{40}\text{S}_{60}$ and $\text{As}_{40}\text{Se}_{60}$ binary glassy layers [1, 5], a phase separation, leading to the formation of a new phase of As_2O_3 (arsenolite) on the surface of the $\text{As}_{40}\text{S}_{40}\text{Se}_{20}$ films, has been found. Thus, the XRD pattern of the representative exposed $\text{As}_{40}\text{S}_{40}\text{Se}_{20}$ film (see figure 2)

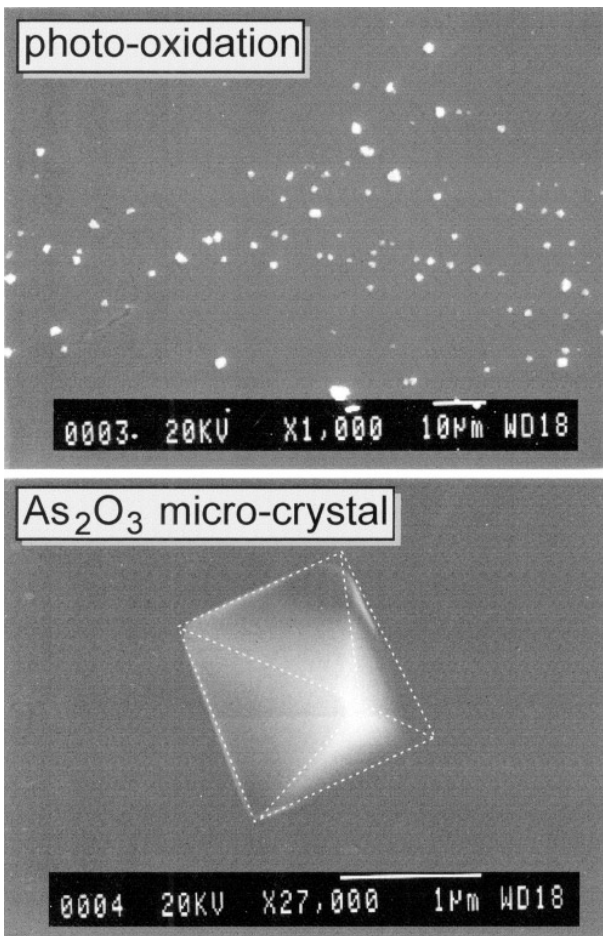


Figure 8. Scanning electron microscope photo-micrograph of the surface of a representative As₄₀S₄₀Se₂₀ amorphous layer, after having been illuminated with UV light for 3 h, under room ambient conditions. An illustrative magnified view of a particular cubic micro-crystal of arsenolite is also displayed.

shows two clear peaks at $2\theta = 14.02^\circ$ and 28.04° (see ASTM card 36-1490). This surface effect is very closely related to the strong optical absorption for high photon energies that the amorphous chalcogenide layers generally exhibit (see figure 6). From the spectral irradiance curve of the Hg arc lamp shown in figure 1, it can be seen that there are high output peaks in the region from about 300 to 450 nm (corresponding to photon energies of around 2.8–4.1 eV). Therefore, a significant part of the radiation emitted by the Hg lamp (the UV part) does not penetrate into the chalcogenide layer. It is the cause of a partial photo-degradation of the film at its surface. As light exposure has been carried out in air, partial photo-oxidation and partial photo-hydrolysis could take place, which would result in the appearance of relatively small, but recognizable arsenic trioxide micro-crystals [1, 5]. The surface morphology of the illuminated samples was carefully observed under the scanning electron microscope, in order to identify these As₂O₃ micro-crystals (see figure 8). Owing to the relatively low concentration of these micro-crystals on the surface (it should be pointed out that figure 8 was taken from a small array with a very unusual high concentration of As₂O₃ crystals), they should not influence significantly the

optical transmission measurements and, therefore, the results obtained from them. Also, it is important to note that no significant compositional changes were found in the exposed samples by energy-dispersive spectroscopy.

4. Conclusions

Amorphous As₄₀S₄₀Se₂₀ chalcogenide films undergo structural transformations when annealed at a temperature near the glass transition temperature (i.e. a thermal-structural transformation), and when exposed to bandgap illumination (i.e. a photo-structural transformation). The disappearance of the FSDP in the XRD pattern has been interpreted as a diminution of the interstitial volume around the As-centred structural units. This result is certainly consistent with the decrease of the film thickness found for the samples whether annealed or illuminated. Also, indications of a photo-oxidation process have been clearly found: arsenic trioxide micro-crystals were unequivocally identified visually by scanning electron microscopy and structurally by XRD measurements.

Changes in the optical properties of the as-evaporated films after thermal annealing near T_g , as well as after bandgap illumination with a Hg arc lamp, have been systematically studied in this work. In particular, the refractive indices of the virgin films increase with either of the two treatments, attaining final values very close to the corresponding bulk-glass values. Another finding is a red shift of the optical absorption edge of the virgin layer, as a consequence of the annealing (a thermal-darkening process has taken place), as well as light exposure (in other words, a photo-darkening effect). Indeed, photo-darkening research on the As₄₀S₄₀Se₂₀ films is still running and the up-to-date results indicate that the annealing-illumination cycle is clearly a reversible process. The detailed results will be published in the near future [38]. As a final point, there is an excellent consistency between our experimental results and those reported in the literature concerning the thermally- and photo-induced phenomena in As₂S₃ and As₂Se₃ binary stoichiometric thin-film glasses.

Acknowledgments

The authors are grateful to Dr A H Moharram (Physics Department, Assiut University, Assiut, Egypt) and to Dr A V Stronski (Institute of Semiconductor Physics, National Academy of Sciences, Ukraine) for the critical reading of the paper, and to Mr Royston Snart for English language assistance. This work was supported by the CICYT (Spain), under the MAT98-0791 project.

References

- [1] Berkes J S, Ing S W and Hillegas W J 1971 *J. Appl. Phys.* **42** 4908
- [2] De Neufville J P, Moss S C and Ovshinsky S R 1973/74 *J. Non-Cryst. Solids* **13** 191
- [3] Pfeiffer G, Paesler M A and Agarwal S C 1991 *J. Non-Cryst. Solids* **130** 111
- [4] Petkov K, Vlcek M and Frumar M 1992 *J. Mater. Sci.* **27** 3281
- [5] Dikova J, Starbov N and Starbova K 1994 *J. Non-Cryst. Solids* **167** 50

- [6] Shpotyuk O I 1994 *Phys. Status Solidi b* **183** 365
- [7] Tichý L, Vidourek A, Nagels P, Callaerts R and Tichá H 1998 *Opt. Mater.* **10** 117
- [8] Prieto-Alcón R, González-Leal J M, Bernal-Oliva A M and Márquez E 1998 *Mater. Lett.* **36** 157
- [9] González-Leal J M, Márquez E, Prieto-Alcón R, Bernal-Oliva A M, Ruiz-Pérez J J and Corrales C 1998 *Mater. Sci. Forum* **287–288** 353
- [10] Nagels P, Tichý L, Sleenckx E and Callaerts R 1998 *J. Non-Cryst. Solids* **227–230** 705
- [11] Kuzukawa Y, Ganjoo A and Shimikawa K 1998 *J. Non-Cryst. Solids* **227–230** 715
- [12] Ovshinsky S R and Fritzsche H 1973 *IEEE Trans. Electron.* **20** 91
- [13] Stronski A V, Romanenko P F, Robur I I, Indutnyi I Z, Shepeljavi P E and Kostyukevich S A 1993 *J. Inf. Rec. Mats.* **20** 541
- [14] Indutnyi I Z, Shepeljavi P E, Romanenko P F, Robur I I and Stronski A V 1996 *Proc. SPIE* **3055** 50
- [15] Swanepoel R 1983 *J. Phys. E: Sci. Instrum.* **16** 1214
- [16] Ramírez-Malo J B, Márquez E, Villares P and Jiménez-Garay R 1992 *Phys. Status Solidi a* **133** 499
- [17] Ramírez-Malo J B, Márquez E, Villares P and Jiménez-Garay R 1993 *Mater. Lett.* **17** 327
- [18] Wagner T and Kasap S O 1996 *Phil. Mag.* **B 74** 667
- [19] Oriol Catalog 1994 *Light Sources, Monochromators, Spectrographs, Detectors and Fiber Optics* vol II (USA: Oriol Corporation) pp 1–42
- [20] Elliott S R 1991 *Nature* **354** 445
- [21] Elliott S R 1991 *Phys. Rev. Lett.* **67** 711
- [22] Elliott S R 1990 *Physics of Amorphous Materials* 2nd edn (London: Longman) p 147
- [23] Moss S C and Price D L 1985 *Physics of Disordered Materials* ed D Adler, H Fritzsche and S R Ovshinsky (New York: Plenum) p 77
- [24] Feltz A, Pohle M, Steil H and Herms G 1985 *J. Non-Cryst. Solids* **125** 271
- [25] Lin C, Busse L E, Nagel S R and Faber J 1984 *Phys. Rev. B* **29** 5060
- [26] Tanaka Ka 1975 *Appl. Phys. Lett.* **26** 243
- [27] Bhatia A B and Thornton D E 1970 *Phys. Rev. B* **2** 3004
- [28] McClain M, Feldman A, Kahaner D and Ying X 1991 *J. Comput. Phys.* **5** 45
- [29] Swanepoel R 1984 *J. Phys. E: Sci. Instrum.* **17** 896
- [30] Wemple S H and Di Domenico M 1971 *Phys. Rev. B* **3** 1338
- [31] Wemple S H 1973 *Phys. Rev. B* **7** 3767
- [32] Solomon I, Schmidt M P, Sénémaud C and Driss Khodja M 1988 *Phys. Rev. B* **38** 13 263
- [33] Tanaka Ke 1980 *Thin Solid Films* **66** 271
- [34] Márquez E, González-Leal J M, Prieto-Alcón R, Vlcek M, Stronski A, Wagner T and Minkov D A 1998 *Appl. Phys. A* **67** 371
- [35] Sanghera J S, Nguyen V Q and Aggarwal I D 1996 *J. Am. Ceram. Soc.* **79** 1324
- [36] Tauc J 1974 *Amorphous and Liquid Semiconductors* ed J Tauc (New York: Plenum) p 171
- [37] Urbach F 1953 *Phys. Rev.* **92** 1324
- [38] Márquez E *et al* 1999 to be published